Transition of Linear Polymer Dimensions from Θ to Collapsed Regime. 1. Polystyrene/Cyclohexane System

I. H. Park, Q.-W. Wang,† and Benjamin Chu*

Department of Chemistry, State University of New York at Stony Brook, Long Island, New York 11794-3400. *Received October 28, 1986*

ABSTRACT: We report the results of a recent light-scattering investigation on several different high molecular weight (M_w ranging from 4×10^6 to 20×10^6 g/mol) polystyrenes in cyclohexane from Θ-temperature to the collapsed state. The temperature (T) dependence of the radius of gyration (R_g) and that of the hydrodynamic radius (R_h) can be represented by master curves in a $\alpha^3|\tau|M_w^{1/2}$ vs. $|\tau|M_w^{1/2}$ plot, where α [$\equiv R(T)/R(\Theta)$] is the expansion factor and τ [$\equiv(T-\Theta)/\Theta$] is the reduced temperature. We were able to observe the collapsed state based on the size changes in the static radius of gyration. However, the dynamic property, i.e., R_h, approaches the collapsed state at a much lower temperature. We also observed that a "metastable" collapsed state could exist for finite (but long) time periods below the cloud-point curve, especially in the very dilute concentration range of high molecular weight ($M_w \geq 17.5 \times 10^6$ g/mol) polystyrenes. A rapid shrink-down of polymer size and subsequent phase separation due to the metastable collapsed state were discussed. The experimental data were compared with previously published results and the blob theory.

I. Introduction

Flory[1] stated a long time ago that the average dimension and conformation of a single polymer chain in solution vary with solvent quality. In a good solvent, the polymer chain expands due to repulsive segment–segment interactions; while in a poor solvent where segment–segment contacts are favored, it can eventually be collapsed to form a globule coil. The transition from random-coil behavior in the Θ state to a globule coil in the collapsed state has been the focus of interest of many theoreticians[2-14] and experimentalists[15-27] for a couple of decades.

There have been controversies among the theoreticians about the existence and the type of coil-to-globule transitions. In addition, the experiments have so far provided conflicting results making definitive conclusions difficult. Some theoreticians[14] who predicted a first-order transition prefer to refer to the experiments reported by Sun et al.[19,20] (referred to as the MIT group) with additional references,[15,23] showing a drastic contraction of the polymer coil in the collapsed state. Another attempt was reported by Bauer and Ullman[17] even though the temperature range studied was far from the collapsed state. Nevertheless, they found that all their experimental data could be fitted to a master curve. Later, many French groups' results (for example, R. Perzynski et al.[24,25] and P. Vidakovic et al.[26]) enforced the existence of a master curve and showed consequently that the transition should be smooth and continuous, rather than discrete, for a sufficiently flexible and long polymer chain. Aside from the difference in the results as reported by the MIT[19] and Prague[23] groups vs. the French groups[24-26] concerning the nature of the coil-to-globule transition for flexible polymer coils in solution, no quantitative agreement exists among the different research groups. Therefore, by studying the polystyrene/cyclohexane (PS/CY) system, we try to reexamine the coil-to-globule transition for flexible polymer coils in solution and to seek plausible sources of those reported discrepancies. It should be noted that Post and Zimm considered the DNA condensation both theoretically[8] and experimentally.[22] The chain stiffness could play a unique role in the coil-to-globule transition, predicting discontinuous behavior for DNA and a diffuse transition for more flexible polymers such as polystyrene.

The theoretical background of coil-to-globule transition and light-scattering technique are summarized in sections II and III, respectively. Experimental conditions and methods of data analysis are described in sections IV and V in order to provide sufficient information concerning the quality of our experiments. Finally, in section VI we present our results and compare them with other experiments and the blob theory.

II. Theoretical Background

Theoretical studies[8,9,28] show that in order to describe correctly the collapsed state of a single polymer chain, a three-body interaction as well as a two-body interaction must be taken into account near and below the Θ-temperature. According to the mean field theory, the expansion factor α and the size R in the collapsed regime have the following relations:

$$\alpha \sim |\tau|^{-1/3}N^{-1/6} \quad \text{(poor solvent)} \tag{1}$$

$$R \sim |\tau|^{-1/3}N^{1/3} \quad \text{(poor solvent)} \tag{2}$$

In the temperature blob theory,[29-31] a polymer chain of N monomers is viewed as a succession of blobs, each containing N_c monomers. The polymer chain obeys Gaussian statistics within each blob. However, the necklace of N/N_c blobs has an expanded structure above the Θ-temperature or a collapsed structure below the Θ-temperature.

The radius of gyration is defined as

$$R_g^2 = (1/N^2)\sum_{n=1}^{N}(N-n)\langle R_n^2\rangle \tag{3}$$

where R_n is the size of a subchain with n monomers and the bracket means an average over all possible configurations of one polymer chain. According to the temperature blob theory, $\langle R_n^2\rangle$ is modeled as

$$\langle R_n^2\rangle = a^2 n \qquad n \leq N_c$$

$$\langle R_n^2\rangle = a^2 N_c^{1-2\nu} n^{2\nu} \qquad n \geq N_c \tag{4}$$

where a is the length of one monomer and ν is an exponent relating the molecular weight with R_g ($\sim M^\nu$). The value of N_c is estimated from the ratio of one monomer volume a^3 to the excluded volume v due to the pair interaction between two monomers, i.e., $N_c \sim (a^3/v)^2$.

As the excluded volume parameter v is proportional to the reduced temperature τ, the temperature blob size N_c

* Author to whom correspondence should be addressed.
† Present address: Department of Chemistry, Peking University, Beijing, People's Republic of China.

0024-9297/87/2220-1965$01.50/0

Table I
Molecular Weights, Polydispersities, Radii of Gyration, and Hydrodynamic Radii in PS/CY at the Θ-Temperature (35 °C)

sample	$M_w \times 10^{-6}$, g/mol	M_w/M_n	R_g, nm[a]	R_h, nm[b]	R_g^2/M_w[c]	R_h^2/M_w[c]	R_h/R_g
x	0.90	1.10	29.8	21.5	9.9	5.1	0.72
2N	1.98	1.10	44.3	33.0	9.9	5.5	0.74
4N	4.57	1.14	67.0	48.7	9.8	5.2	0.73
8N	8.62	1.26	95.3	69.5	10.5	5.6	0.73
17B	17.5	2.1	167	110	15.9	6.9	0.66
x[e]	24.7	~2	196	136	15.6	6.6	0.69
F-1[d]	11.3	1.3	114		11.5		
F-2[d]	17.7	1.5	151	105	12.9	6.2	0.70
F-3[d]	10.5	1.4	112	79.9	11.9	6.1	0.71

[a] R_g could be determined to about ±3%. [b] R_h could be determined to about ±2%. [c] Unit = 10^{-18} cm² mol/g. [d] The F series was fractionated from the sample 17B. [e] In the presence of 1 wt % antioxidant, Θ = 32.7 °C.

becomes $N_c = A^*/\tau^2$, with A^* being a dimensionless proportionality constant, depending only weakly on the nature of the solvent[29] and the monomer structure. The value of R_g at the Θ-temperature is $R_g(\Theta) = aN^{1/2}/6$. The expansion factor α_s of the radius of gyration, defined by $\alpha_s = R_g(x)/R_g(\Theta)$ is

$$\alpha_s = 1.161(N/N_c)^{-1/6} \quad \text{(poor solvent)} \qquad (5)$$

in the poor solvent limit, with $\nu = {}^1/_3$ and $x = N_c/N$.

The hydrodynamic radius R_h of a polymer chain is defined by

$$R_h = k_B T/(6\pi\eta_0 D_0) \qquad (6)$$

where η_0 is the solvent viscosity and D_0 is the translational diffusion coefficient at infinite dilution. On the basis of temperature blob model of eq 4 and in the poor solvent limit with $\nu = {}^1/_3$,

$$\alpha_h = 1.481(N/N_c)^{-1/6} \quad \text{(poor solvent)} \qquad (7)$$

$$R_h = 0.402aN^{1/3}N_c^{-1/6} \quad \text{(poor solvent)} \qquad (8)$$

Although there have been disagreements among theoreticians about the existence and the type of the coil-to-globule transition for one single polymer chain in solution, we can extract some characteristic properties in the collapsed regime.[10,25]

(1) The monomer density inside the polymer coil is uniform, independent of the polymer molecular weight.

(2) The radius (either static or hydrodynamic) of the collapsed coil is scaled as $N^{1/3}|\tau|^{-1/3}$.

(3) $\alpha_s^3|\tau|N^{1/2} \sim$ constant and $\alpha_h^3|\tau|N^{1/2} \sim$ constant, but these two constants are not the same.

III. Laser Light Scattering

The coil-to-globule transition of a single polymer chain in solution is accompanied by a dimensional contraction of the single polymer chain from the Θ-temperature to a collapsed temperature within a very narrow concentration gap between infinite dilution and the left side of the coexistence curve. The transition can be observed only at very dilute concentrations, because the collapsed state must be realized before the onset of phase separation. Laser light scattering is an appropriate technique for studying the coil-to-globule transition.

IIIa. Static Light Scattering.[32] For a polydisperse polymer solution in the absence of intermolecular interactions, the polarized (excess) Rayleigh ratio R_{vv} (cm^{-1}) in dilute solution has the form

$$HC/R_{vv} = (1/M_w)P^{-1}(K) + 2A_2C \qquad (9)$$

where H, C, M_w, P, K, and A_2 are, respectively, an optical constant, concentration, weight-average molecular weight, particle scattering factor, magnitude of momentum transfer vector, and second virial coefficient. Equation 9 is used to determine M_w, A_2, and R_g.

IIIb. Dynamic Light Scattering.[33-35] In quasi-elastic light scattering, the intensity–intensity time correlation function $\langle I(0)I(t)\rangle = G^{(2)}(t)$ can be expressed in terms of the normalized electric field correlation function $g^{(1)}(t)$

$$G^{(2)}(t) = A(1 + b|g^{(1)}(t)|^2) \qquad (10)$$

where A and b are, respectively, the base line and the coherence factor of the spectrometer, and $g^{(1)}(t) = \langle E^*(0)E(t)\rangle/\langle E^*(0)E(0)\rangle$ with E being the scattered electric field.

For polydisperse particles with or without internal motions

$$|g^{(1)}(t)| = \int_0^\infty G(\Gamma)e^{-\Gamma t}\,d\Gamma \qquad (11)$$

where $G(\Gamma)$ is the normalized characteristic line width distribution function. The cumulants method can be used to retrieve information on $G(\Gamma)$ for narrow characteristic line width distributions.[36]

$$\ln|g^{(1)}(t)| = -\bar{\Gamma}t + (1/2)(\mu_2/\bar{\Gamma}^2)(\bar{\Gamma}t)^2 + \ldots \qquad (12)$$

where $\bar{\Gamma} = \int_0^\infty G(\Gamma)\,d\Gamma$, $\mu_2 = \int_0^\infty(\Gamma - \bar{\Gamma})^2G(\Gamma)\,d\Gamma$, with $\bar{\Gamma}$ and μ_2 being respectively the average characteristic line width and the second central moment, and VAR = $\mu_2/\bar{\Gamma}^2$. We can express $\bar{\Gamma}$ at finite K and finite C approximately as

$$\bar{\Gamma}/K^2 \cong \bar{D}_0(1 + fK^2\langle R_g^2\rangle_z)(1 + k_dC) \qquad (13)$$

where $\bar{D}_0$, k_d, and f are respectively the z-average translational diffusion coefficient at infinite dilution, the second virial coefficient for diffusion, and a dimensionless constant that depends upon chain structure, polydispersity, and solvent quality.[37] The subscript zero denotes infinite dilution. According to Brown et al.,[38] $\mu_2/\bar{\Gamma}^2 \sim (1/4)(M_z/M_w - 1)$ if $M_z/M_w < 1.25$.

IV. Experimental Section

In view of the differences between our experimental data and some of those results reported in the literature, we describe in detail how our polymer solutions were prepared and polymer samples fractionated and characterized and possible degradation by laser radiation at extremely dilute concentrations.

IVa. Sample Preparation. Polystyrene samples were used without further fractionation except the $M_w = 20 \times 10^6$ g/mol sample (17B) from Pressure Chemical Co. The specifications of the polymer samples used in this study are listed in Table I. Some fractionated samples were prepared by fractional precipitation, in which the polymer (17B) was dissolved in a benzene–methanol mixture (75:25 by volume) and the solution was cooled in steps from 35 to 28 °C. For purification of solvent, cyclohexane was kept in a molecular sieve (4 Å) and distilled under P_2O_5 just before use. We first prepared a mother solution with a concentration of $\sim 5 \times 10^{-4}$ g/g. After wrapping the stopper of the mother solution bottle with Teflon tape and Parafilm, we put it into a

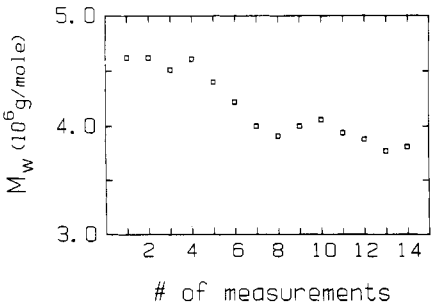

Figure 1. Degradation of polymer chain due to high laser power density in the PS/CY system (sample 4N, $M_w = 4.6 \times 10^6$ g/mol, $C = 2.5 \times 10^{-6}$ g/g, $T \sim 35$ °C, and $\lambda_0 = 514.5$ nm). Each set of measurements consists of a ~30-min exposure at a laser power density of $\sim 1 \times 10^2$ W/cm^2 for the absolute scattered intensity data and less than 1-h exposure at a laser power density of $\sim 6 \times 10^2$ W/cm^2 for the line-width data. Incident beam volume/solution volume is $\sim 1 \times 10^{-3}$.

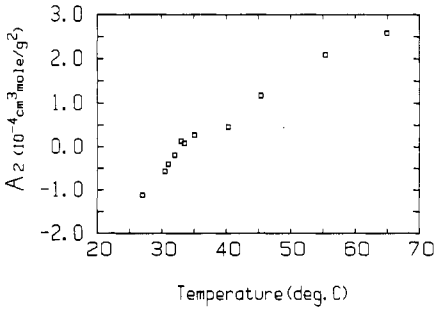

Figure 2. Variation of second virial coefficient A_2 as a function of temperature (°C) in the polystyrene ($M_w = 2.33 \times 10^5$ g/mol)/cyclohexane system with 1 wt % antioxidant (2,6-di-*tert*-butyl-4-methylphenol). The Θ-temperature of the PS/CY (1 wt %) system could be estimated to be 32.7 °C.

small desiccator in an oven with temperatures set at ~45 °C. For high molecular weight polymer samples, complete dissolution requires a minimum of a couple of days with occasional stirring. Complete dissolution for high molecular weight polymers such as polystyrene in cyclohexane takes time. We were careful to check the absolute scattered intensity of very dilute polymer solutions. Reproducible intensity results from different preparations confirm the same molecular weight as calibrated by good solvent and thus complete dissolution. Next, the mother solution was diluted 20–100 times to the measured concentration, which is on the order of $CM_w \sim 20$ g^2 cm^{-3} mol^{-1}. This minimum concentration corresponds to a C/C^* value of (1–2) $\times 10^{-4}$, where the overlap concentration C^* can be taken as $C^* \sim 40/M_w^{1/2}$ (g/cm^3) for the PS/CY system[25] with M_w expressed in units of g/mol.

IVb. Characterization of System. IVb.1. Polydispersity of Polymer. The index of polydispersity (e.g., M_w/M_n, M_z/M_w, and variance) of our polystyrene samples used in this study is listed in Table I. The figure part in the sample code denotes roughly the weight average molecular weight by units of 10^6 g/mol. The subsequent alphabet "B" or "N" stands for the broad or narrow polydispersity. A polydispersity of $M_w/M_n = 1.3$ was used as the borderline distinguishing the narrow and broad polydispersity. Usually, samples with M_w higher than 10^7 g/mol had a broad polydispersity.

IVb.2. Degradation of Polymer. At very low polymer solution concentrations ($C < 10^{-5}$ g/g), even a small absolute amount of polymer degradation has serious effects on the molecular weight and size determinations. For instance, absolute degradation of 1×10^{-6} g of polymer corresponds to a 10% weight fraction change in 1 g of polymer solution at $C = 10^{-5}$ g/g. However, such degradation can always be neglected at ordinary concentrations ($C > 10^{-3}$ g/g). Although we are not interested in the detailed mechanisms of polymer degradation, we examined carefully several possible causes of degradation, such as high laser power density, trace of oxygen, and weak chemical bonds in the long polymer chain. We first investigated the effect when a very dilute polymer solution was exposed to a high power density laser beam (~1 W/(0.04 cm)^2 or ~625 W/cm^2). As shown in Figure 1, the absolute scattered intensity of the polymer solution (sample 4N, $C = 2.5 \times 10^{-6}$ g/g) decreased by ~18% after 14 sets of measurements at 514.4 nm, where each set took ~30 min of exposure at ~100 W/cm^2 for the absolute scattered intensity data and less than 1 h at ~600 W/cm^2 for the line-width data. In actual experiments, this difficulty could be alleviated by degassing the oxygen in the polymer solution, by using a lower power density laser beam (less than ~100 W/cm^2), and by reducing unnecessary exposure of the polymer solution to laser radiation during our studies.

IVb.3. Θ-Temperature. For the PS/CY system, Θ = 35 °C. The Θ-temperature of PS/CY systems with 1 wt % antioxidant was measured experimentally. Figure 2 shows plots of the second virial coefficient A_2 vs. temperature for polymer solutions in the presence of a known amount of antioxidant. In these plots, the temperature at which $A_2 = 0$ was defined as our Θ-temperature for that system. The Θ-temperature of the PS/CY system with 1 wt % antioxidant (denoted as PS/CY (1 wt %)) was estimated to be 32.7 °C, 2.3 deg lower than the Θ-temperature for polystyrene in cyclohexane.

IVc. Physical Constants. The reference values of (dn/dC) at 35 °C for the PS/CY system were respectively[39] 0.1810 and 0.1695 cm^3/g at $\lambda_0 = 436$ and 546 nm. The temperature coefficient of $(dn/dC)_T$ was 2.85×10^{-4} cm^3/(g deg).[39] We used benzene as a reference for computing the Rayleigh ratio R_{vv} with $R_{vv}^{BZ} = 2.49 \times 10^{-5}$ and 3.20×10^{-5} cm^{-1} at 25 °C for benzene at $\lambda_0 = 514.5$ and 488 nm, respectively. The temperature dependence of R_{vv}^{BZ} for benzene was given[40]

$$R_{vv}^{BZ}(T) = R_{vv}^{BZ}(25\ °C)[1 + (3.68 \times 10^{-3})(T - 25\ °C)] \quad (14)$$

where $R_{vv}^{BZ}(T)$ is the Rayleigh ratio of benzene at temperature T (°C). The viscosities of solvent cyclohexane were calculated by using eq 15,[41] where η_0 (cP) is the solvent viscosity at temperature T expressed in degrees Celcius.

$$\eta_0 = (6.1739 \times 10^{-3}) \exp[1481.6/(T + 273)] \quad (15)$$

V. Methods of Data Analysis

For large polymer coils in solution, the $KR_g < 1$ range is often difficult to achieve experimentally. We describe our empirical approach to determine R_g and R_h by taking into account higher order interference effects, finite concentrations, and acceptable deviation from single-exponential correlation function profile analysis.

Va. Intensity Data. As our experiments were performed at extremely dilute concentrations ranging from 10^{-5} to 10^{-6} g/g, the correction to finite concentration in the determinations of M_w and R_g would be less than 1% ($A_2CM_w \sim (3 \times 10^{-5})(4 \times 10^{-5})(4.6 \times 10^6) \sim 0.5\%$ even at very low temperatures and could be taken to be negligible. Here, a value of $\sim 3 \times 10^{-5}$ mol cm^3/g^2 for A_2 used in the above calculation was approximated from Figure 2. That value for A_2 is an overestimate because of much higher molecular weight PS samples used in the actual studies. Furthermore, we usually used measurements of two different concentrations in the very dilute solution regime in order to assure ourselves that effects of intermolecular interactions are negligible.

In a plot of HC/R_{vv} vs. $\sin^2(\theta/2)$, the radius of gyration can be computed from the initial slope where $KR_g < 1$. If a wide range of scattering angle is used to measure the slope at $KR_g \gtrsim 1$, the initial slope approach is no longer applicable. We used an empirical combination of Zimm and Berry plots at different ranges of KR_g in order to ascertain a credible determination of R_g.

Polydispersity could be estimated from scattered intensity measurements. Miyaki et al.[42] were able to determine the polydispersity of very high molecular weight polymers. The index of polydispersity of our high molecular weight polystyrene sample obtained by using the Fujita plot is listed in Table I.

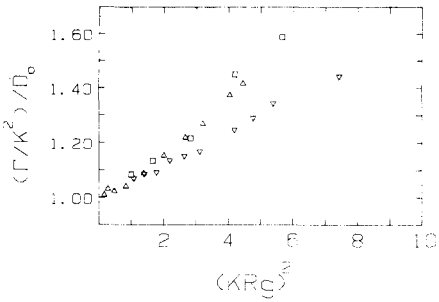

Figure 3. Variation of $\bar{\Gamma}_N/K^2$ [$\equiv(\bar{\Gamma}/K^2)/\bar{D}_0$] as a function of KR_g: (△) sample 4N ($M_w = 4.6 \times 10^6$ g/mol, $M_w/M_n = 1.14$); (□) sample 8N ($M_w = 8.6 \times 10^6$ g/mol, $M_w/M_n = 1.26$); (▽) sample 17B ($M_w = 17.5 \times 10^6$ g/mol, $M_w/M_n = 2.1$). Values of $(\bar{\Gamma}/K^2)/\bar{D}_0$ for PS samples (4N, 8N) with narrow molecular weight distribution show a strong upturn trend with respect to increasing KR_g values. $\bar{D}_0$ is the translational diffusion coefficient at zero scattering angle.

Vb. Line-Width Data. The z-average characteristic line width $\bar{\Gamma}$ in this experiment was calculated by the second-order cumulants fitting method. The difference between $\bar{\Gamma}$ values obtained by the second- and third-order cumulants fitting procedure usually agreed to within 2–3% in sample 17B ($M_w/M_n = 2.1$). The deviation plots show almost no difference between the second- and third-order cumulant fits.

The finite concentration effect in our measurements of $\bar{\Gamma}$ could also be shown to be negligible, e.g., for sample 4N ($k_dC \sim 100(4 \times 10^{-5}) \sim 0.4\%$). The above-used value of k_d was estimated from well-established empirical relations at Θ-temperature ($k_d = 0.052M_w^{1/2}$ cm^3/g in PS/CY).[26] According to theoretical calculations, the f value becomes 0.173 for a linear monodisperse Gaussian chain. It implies that $\bar{\Gamma}/K^2$ measured even at $KR_g = 1$ deviates by 17% from the true translational diffusion coefficient. We plotted the normalized $\bar{\Gamma}_N/K^2$ [$=(\Gamma/K^2)/\bar{D}_0$] as a function of $(KR_g)^2$. In Figure 3, a very narrow polydisperse sample 4N showed a strong upturn but for polydisperse sample 17B; a straight line was obtained up to $(KR_g)^2 \sim 4$.

The condition for $KR_g < 1$ can be fulfilled easily at ordinary low scattering angles ($\theta \sim 20°$) for low molecular weight samples such as 4N. Then the translational diffusion coefficient could be obtained without extrapolation to $K = 0$. However, at times it was difficult to obtain the condition for $KR_g < 1$ with large molecular weight sample 17B because of the presence of dust particles. By using the linearity condition between $\bar{\Gamma}/K^2$ and $(KR_g)^2$, we could extrapolate the data points above $KR_g > 1$ into the zero scattering angle limit without introducing appreciable errors. All polydispersity results are listed in Table I. It is interesting to note that the variance of narrow molecular weight distribution samples (e.g., 4N) increases rapidly with increasing KR_g values, but that of polydisperse sample (e.g., 17B) increases very little.

VI. Results and Discussion

VIa. Effect of Polydispersity on Polymer Dimension. We used the size of our polymer samples measured at the Θ-temperature as a reference standard for the unperturbed polystyrene coil which is well established in the literature. The z-average sizes (R_g and R_h) at the Θ-temperature and the scaling constants[2] such as R_g^2/M_w and R_h^2/M_w have been summarized in Table I and elsewhere.[43] In a log–log plot of chain size vs. molecular weight, all our data could not be scaled with a typical exponent of 0.5 based on the ideal chain behavior. Some data for high molecular weight samples, such as 17B etc., deviated from the 0.5 value for the slope, as shown in Figure 4. We believe that the deviation (in R_g value by more than 20%)

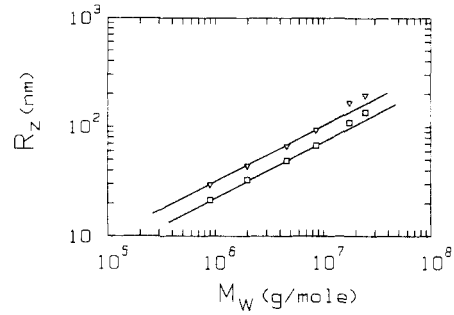

Figure 4. log–log plots of z-average size (R_g and R_h) vs. weight-average molecular weight at the Θ-temperature: (▽) R_g; (□) R_h. Solid lines denote a typical exponent of 0.5 based on the ideal chain behavior. High molecular weight samples showed measurable deviations from the 0.5 slope, possibly due to increasing polydispersities at higher molecular weights. Θ-Temperatures of the PS/CY system and the PS/CY (1 wt %) system are 35 and 32.7 °C, respectively.

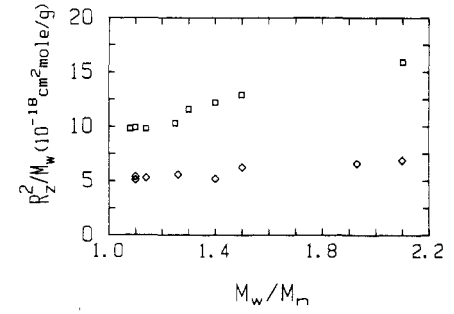

Figure 5. Variation of scaling constant (R_z^2/M_w) as a function of the index of polydispersity (M_w/M_n) at the Θ-temperature: (□) $R_z^2 = R_g^2$; (◇) $R_z^2 = R_h^2$. Scaling constant increase with increasing index of polydispersity. Θ-Temperatures of the PS/CY system and the PS/CY (1 wt %) system are 35 and 32.7 °C, respectively.

is beyond our experimental error limits. As illustrated in Figure 5, the scaling constant appeared as a monotonically increasing function with respect to the index of polydispersity. Thus, polydispersity seems to be the source of the observed deviation. It can be expected that the contribution of molecular weight distribution (MWD) to z-average quantities is different from that of MWD to weight-average quantities and that z-average quantities are much more sensitive to the high molecular weight fraction than weight-average quantities. Here, the physical quantities (R_g^2 and $\bar{D}_0$) are z-averaged but the molecular weight as observed by light scattering is weight-averaged. Therefore, the scaling relation can be applied only to a homologous series of narrow MWD ($M_w/M_n < 1.2$) polymers. If the polymer samples are polydisperse, it is necessary that each polymer sample has at least the same polydispersity index. The scaling constant for polydisperse polymer systems is no longer the same as that for the monodisperse system. There exists a possibility of estimating the polydispersity index from the change in the scaling constant as a result of polymer polydispersity. An average value [9.8×10^{-18} cm^2 (mol/g)] of R_g^2/M_w for narrow MWD polystyrene samples (2N, 4N, etc.) showed a better agreement with the value [9.36×10^{-18} cm^2 (mol/g)] of Outer et al.[44] than those values reported by others.[42,45] From line-width measurements, our value [5.2×10^{-18} cm^2 (mol/g)] of R_h^2/M_w was in agreement with the reference value of 5.24×10^{-18} cm^2 (mol/g).[45] In Figure 5, it was also observed that the variation of R_g^2/M_w with the index of polydispersity was much larger than that of R_h^2/M_w.

The most serious experimental problem in studying the coil-to-globule transition is that there exists the possibility

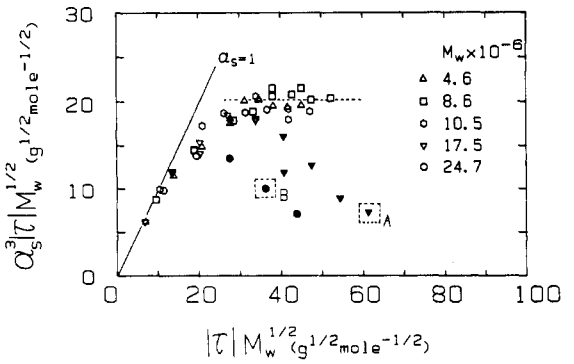

Figure 6. Variation of the scaled expansion factor $\alpha_s^2|\tau|M_w^{1/2}$ of static size as a function of scaled reduced temperature $|\tau|M_w^{1/2}$. $\alpha_s^3|\tau|M_w^{1/2}$ at the asymptotic plateau region (denoted by a dashed line) is 20.1 $g^{1/2}$ $mol^{-1/2}$. Filled symbols indicate "metastable" collapsed regime. Data are listed in ref 43. It should be noted that the scaled curve was obtained by using PS with different molecular weights and at different concentrations.

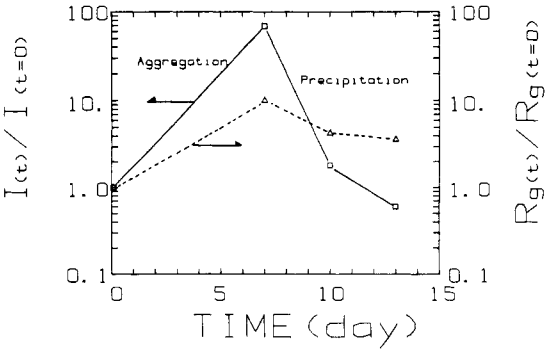

Figure 7. Variation of scattered intensity and radius of gyration of one metastable collapsed state (point A in Figure 6) with time (day). The initial state at time $t = 0$ was denoted as point A (17B, $M_w = 17.5 \times 10^6$ g/mol, $C = 1.8 \times 10^{-6}$ g/g, at 30.5 °C) in Figure 6. I denotes the scattered intensity extrapolated to zero scattering angle: (□) scattered intensity ratio; (△) ratio of radius of gyration.

of fractional phase separation, if the polydisperse polymer solution at finite concentration is cooled down much below the Θ-temperature. Generally, the broader the MWD, the narrower the accessible (thermodynamically stable) temperature range becomes.

In coil-to-globule transition studies, polydispersity would prevent our polymer solutions from reaching the globule regime because of fractional precipitation at finite concentrations.

VIb. Static Size. VIb.1. One-Phase Stable Region. The scaled expansion factor $\alpha_s^3|\tau|M_w^{1/2}$ was plotted as a function of the scaled reduced temperature $|\tau|M_w^{1/2}$ where the collapsed state was observed as a plateau region and $\alpha_s = R_g(T)/R_g(\Theta)$. After examining our data in Figure 6, we could classify the results into several regimes such as the Θ-regime, the cross-over regime, the collapsed regime, and the metastable collapsed regime. In the range $0 < |\tau|M_w^{1/2} < 10$, there exists a Θ-regime with the slope of $\alpha_s \sim 1$ where the polymer chain remains essentially unperturbed. Our data agree with literature results in the Θ-regime. After the Θ-regime, the $\alpha_s^3|\tau|M_w^{1/2}$ values begin to deviate from the $\alpha_s = 1$ line and above $|\tau|M_w^{1/2} \sim 30$, reach the plateau region corresponding to the collapsed state. Some cross-over behavior was observed between the Θ-regime and the collapsed regime with $10 < |\tau|M_w^{1/2} < 30$. Unusual data points (denoted by filled symbols in Figure 6) appeared over the whole temperature range. We shall refer to those points as the "metastable" collapsed regime. All our experimental data except those points in the metastable state could be represented by one master curve. The universality of polymer coil contraction in the coil-to-globule transition has already been demonstrated by other authors.[17,24-26] Our experimental data differ from most literature results in the details on how the plateau region is reached, the magnitude of coil size in the globule state, and whether the PS/CY system is at stable equilibrium in the globule regime. A log–log plot of the expansion factors α_s and α_h in the thermodynamically stable one-phase state versus the scaled reduced temperature showed a slope of -0.31 ± 0.03 for α_s in the asymptotic limit, in very good agreement with the theoretical exponent of $-1/3$ in eq 1. The rate of change of α_h suggests that we have almost reached the collapsed regime on the basis of R_h.

On the basis of static R_g values, the collapsed state was observed conclusively above $|\tau|M_w^{1/2} > 30$. The asymptotic height of $\alpha_s^3|\tau|M_w^{1/2}$ in the plateau region was about 20.1 $\pm$ 0.8 $g^{1/2}$ $mol^{-1/2}$. In the collapsed regime, the monomer density distribution inside each polymer coil becomes essentially uniform after only a ~15% contraction from the ideal Gaussian coil behavior, in contrast with most reported larger magnitudes of contraction in the globule state.

All data points which belong to the metastable collapsed regime appeared below the master curve in Figure 6. This means that the radii of gyration of those data points contracted more than the values predicted by the master curve. The size could not be scaled with reduced temperature by using an exponent of $-1/3$ even after the scaled reduced temperature $|\tau|M_w^{1/2}$ reached the collapsed regime. For example, the data points of sample 17B near the asymptotic height with $\alpha_s^3|\tau|M_w^{1/2}$ (~18.5) fell below the value (~20) at the plateau region and decreased with decreasing temperature.

To summarize, in the thermodynamically stable one-phase state: (1) α_s and α_h can be represented by master curves; (2) for α_s, the plateau region was reached with $\alpha_s^3|\tau|M_w^{1/2} \sim 20$ $g^{1/2}$ $mol^{-1/2}$ and a scaling exponent in the globule regime of ~1/3; (3) the contraction was only ~15%, much smaller than most reported in the literature.

VIb.2. Metastable Region. We checked, first, whether or not the data as denoted by filled symbols in Figure 6 were really thermodynamically stable. The scattered intensities of data points always increased overnight at the given temperature. A more detailed investigation was performed at one point (denoted as "A" in Figure 6, sample 17B, $C = 1.8 \times 10^{-6}$ g/g at 30.5 °C) in the "metastable" collapsed regime. As shown in Figure 7, the scattered intensity reached a maximum value after 7 days and the increase could amount to more than 100 times the initial scattered intensity at the same given temperature (30.5 °C). The polymer chain also reached a maximum size at the time of maximum intensity. Then both the intensity and the size decreased gradually.

The electric field time correlation functions in Figure 8 show us clearly the tremendously increased sample time (~10^3 times) needed in order to cover the frequency range of the time correlation function after 7 days. On the basis of these observations, we speculate that the polymer chain started to aggregate slowly for 7 days and that the aggregated clusters began to precipitate eventually after reaching a certain size. The growth and precipitation took a very long time because of the extremely dilute concentrations on the left side of the cloud-point curve for very high molecular weight PS/CY systems.

We should now consider possible effects such as critical phenomena, which might influence the coil-to-globule transition. As the dilute polymer solution approaches the cloud-point curve, the critical scattering at finite concen-

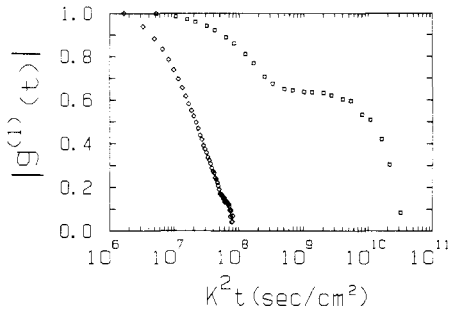

Figure 8. Variation of normalized time correlation function $|g^{(1)}(t)|$ of one metastable collapsed state. The initial state at time $t = 0$ was shown as point A in Figure 6: (◇) at time $t = 0$; (□) after 7 days. The time correlation functions were measured at $\theta = 24°$, $\lambda_0 = 514.5$ nm, and 30.5 °C. The electric field time-correlation function showed a tremendously increased delay time in order to cover the whole frequency range and a distorted shape after 7 days.

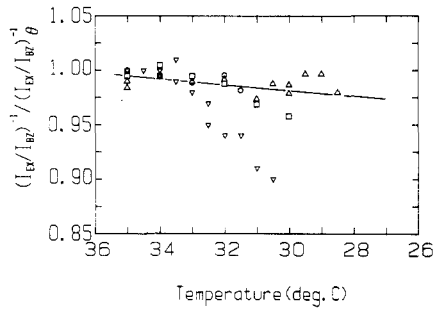

Figure 9. Normalized scattered intensity vs. temperature (°C): (△) sample 4N, $M_w = 4.6 \times 10^6$ g/mol; (□) sample 8N, $M_w = 8.6 \times 10^6$ g/mol; (○) sample F-3, $M_w = 10.5 \times 10^6$ g/mol; (▽) sample 17B, $M_w = 17.5 \times 10^6$ g/mol. Solid line denotes the calculated temperature coefficient (~0.2%/°C) of the normalized inverse scattered intensity on the basis of eq 9. I_{EX} and I_{BZ} are, respectively, the excess scattered intensity of PS/CY solution and the scattered intensity of benzene as a reference.

trations (but away from the critical solution concentration) can be expressed as[46]

$$\lim_{K\to 0} I_c^{-1} \sim \left(\frac{T}{T_{sp}} - 1\right)^{\gamma} \qquad (16)$$

where I_c is the additional scattered intensity introduced by critical effects, T_{sp} is the spinodal temperature in kelvin, and γ (~1.24) is a critical exponent. Here, T_{sp} is a function of polymer concentration. High molecular weight polymer solutions exhibit very asymmetric coexistence curves and the temperature gap between the coexistence curve and the spinodal curve becomes very large in this low concentration range ($C < 10^{-5}$ g/g) for our polymer solutions. Therefore, the additional scattered intensity (or increase of the apparent radius of gyration) due to critical effects could not contribute appreciably to I_c (or R_g) because $T_{sp}(C) \ll T(C)$ where $T_p(C)$ is the phase separation temperature at concentration C. Figure 9 shows the variation of the scattered intensity at zero scattering angle with respect to the temperature. In order to make a proper comparison among intensities scattered by different samples, we normalized all scattered intensities at different temperatures with that at the Θ-temperature. The decrease of inverse scattered intensity of samples 4N and 8N is in good agreement with that calculated from standard temperature coefficients of the physical parameters used in eq 9 (given as a solid line in Figure 9). Thus, we believe that critical phenomena did not play an appreciable role, at least for those data points represented by the master

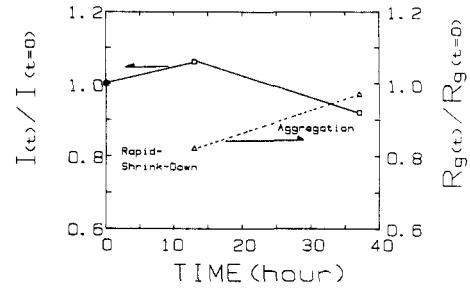

Figure 10. Variation of scattered intensity and radius of gyration of another metastable collapsed state (point B in Figure 6) with time (hour). The initial state at time $t = 0$ was denoted as point B ($M_w = 24.7 \times 10^6$ g/mol, $C = 2.1 \times 10^{-6}$ g/g, at 31 °C) in Figure 6: (□) scattered intensity ratio; (△) ratio of radius of gyration. $I(t)$ is the scattered intensity extrapolated to zero scattering angle at time t. No guideline was drawn in the rapid shrink-down portion of the radius of gyration because the exact path is not obvious.

curve. For sample 17B and at $C = 1.8 \times 10^{-6}$ g/g, the inverse scattered intensity dropped rapidly for $T < 32.5$ °C, which corresponded to the temperature where $\alpha_s^3|\tau|M_w^{1/2}$ reached a peak value in Figure 6.

If we assume that the additional scattered intensity comes from local concentration fluctuations in the homogeneous one-phase region, it conflicts with the abrupt increase in the scattered intensity and the subsequent rapid contraction of the polymer coil. Another possibility is fractional separation, especially if the high molecular weight polymer is sufficiently polydisperse. Then some high molecular weight polymer fractions could precipitate, and only low molecular weight polymer fractions remained in the solution. After fractionation and precipitation of the high molecular weight polymer, the measured apparent radius of gyration could be smaller than the original value before precipitation. However, fractional separation could explain only the eventual small particle size at equilibrium, but could not account for the initial higher scattered intensity. One more point (denoted as "B" in Figure 6 $M_w = 24.7 \times 10^6$ g/mol, $C = 2.1 \times 10^{-6}$ g/g at 30 °C) was chosen to study the time dependence of scattered intensity and polymer (or cluster) size as shown in Figure 10.

After 13 h, the size of the polymer chain was contracted by ~20% while the absolute scattered intensity increased by ~5%. In Figure 10, the initial decrease in the apparent size of polymer chain and the increase in the apparent molecular weight with increasing time could possibly be attributed to a combination of aggregation and (more dominating) contraction. The subsequent decrease in the absolute scattered intensity and the corresponding polymer size might come mainly from precipitation of aggregated polymers which reduced the overall polymer concentration in the scattering volume and the aggregated (but not yet precipitated) polymer in solution, respectively. In fact, aggregation and precipitation occurred almost simultaneously.

In the metastable regime, we can divide the time domain into two regimes. Initially, intramolecular attractive interaction could play a dominant role because the polymer coil contracts with decreasing temperature. However, over a longer time scale, polymer coils aggregated to form clusters due to intermolecular attractive interactions leading toward phase separation. If the two time domains are strongly coupled, the collapse of each polymer chain and the aggregation of polymer chains occur almost at the same time.

Cuniberti et al.[47] reported that phase separation could be achieved by two different mechanisms. For one mechanism the polymer solution is phase separated by

progressively growing clusters. The other is based upon, first, formation of solidlike dense particles and then coalescence of these particles. Here, we will refer to the former as the growing cluster mechanism and the latter as the compact particle coalescence mechanism. Finally, they concluded that the mechanisms are dependent upon the nature of the chemical system and gave examples such as the PS/CY system for the growing cluster mechanism and the polyacrylic acid/methyl ethyl ketone system for the compact particle coalescence mechanism. The phase-separation mechanism of our metastable collapsed data suggests that the PS/CY system seems to come closer to the compact particle coalescence mechanism.

More importantly, the mechanism of phase separation depends upon the thermodynamic state, i.e., metastable vs. unstable regions. The degree of coupling of the two time domains of intra- and intermolecular attractive interactions could be different in the unstable region when compared with that in the metastable region. For filled symbols, the data represent only the metastable two-phase region. Furthermore, for the filled symbols in Figure 6, the observed values change slowly with time, indicating an absence of stable equilibrium even if it could take days or weeks to detect such observable changes. Thus, for high molecular weight flexible coils such as those exhibited by points A and B in Figure 6, we are not dealing with discontinuous behavior[8,22] in the coil-to-globule transition.

Recently, de Gennes[48] calculated the time scale of a collapse process for a flexible coil with N segments, when a polymer chain is transferred abruptly from Θ-point to poor solvent (e.g., by a shift of temperature ΔT). By his calculation for the PS ($M_w = 10^7$g/mol)/CY system, the collapsed time is generally only on the order of milliseconds. Therefore, in order to separate the two time domains, we should slow down the intermolecular attractive interaction effect either by increasing the distance between polymer chains or by using a very viscous solvent. If we try to compare the distance between polymer chains in our system ($M_w = 17.5 \times 10^6$ g/mol, $C = 1.8 \times 10^{-6}$ g/g) and the PS/CY system reported by Cuniberti et al. ($M_w = 4.23 \times 10^5$ g/mol, $C = 1.0 \times 10^{-3}$ g/g), the average distance in our system ($\sim 2.5 \times 10^{-4}$ cm) is larger by 28 times than that ($\sim 8.9 \times 10^{-6}$ cm) reported by Cuniberti et al. If the collision of polymer chains is controlled by the translational diffusion coefficient, the time for traveling this average distance in our system would be 2300 times longer. This time difference could be the reason why we observe the compact particle coalescence mechanism instead of the growing cluster mechanism under the metastable collapsed regimes which we investigated. It should also be noted that our studies in the metastable collapsed regime were based upon high molecular weight polystyrene samples (17B, etc.) with fairly broad MWD.

To summarize, we attribute the metastable collapsed regime as due to broad MWD ($M_w/M_n = 1.7$–2.1) with the cloud-point curve being located very close to the infinite dilute solution limit. There is fractional separation even at small ΔT. By using the high molecular weight ($M_w \geq 17.5 \times 10^6$ g/mol) polystyrene samples, there is a very wide metastable region below the cloud-point curve with $T_{sp}(C) \ll T_p(C)$, even if the polymer solution concentration is only slightly lower than the critical solution concentration. Thus, it is unlikely that we reached the unstable two-phase region in our experiments. As strong attractive interactions exist in the metastable region, the polymer chain collapses into the compact size very quickly (perhaps within a few milliseconds) but the solution eventually becomes phase separated (very slowly) because of the extremely dilute

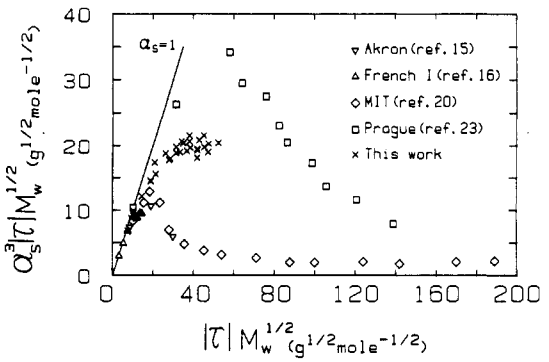

Figure 11. Comparison of our static size data (×) with reference data. Only data points that can be represented by the master curve in Figure 6 were presented.

polymer solution concentration used in our studies. Time-dependent changes of observed values, no matter how slow, further strengthen our supposition that we are not dealing with one-phase stable thermodynamic states for those data not represented by the master curve.

VIb.3. Comparison of Our Experimental Data with Literature Results. Now, we compare our static size data with all known published results in Figure 11. Here, we present only those of our data points (in the one-phase thermodynamically stable region) which can be represented by the master curve. Surprisingly, results by all other groups except those by French I group[16] showed similar patterns in the cross-over and "globule" regimes, in agreement with our data points in the metastable region in Figure 6, *not* our globule region. The literature data can be characterized as follows: (i) only the MIT[19] and the French I groups observed the collapsed regime based on R_g. However, the plateau region of the MIT group had a very small asymptotic height ($\alpha_s^3|\tau|M_w^{1/2} \sim 3$ in contrast to our observed value of ~ 20) and the temperature range of the collapsed regime measured by the French I group was somewhat narrow to be regarded as a definitive observation; (ii) the R_g data measured by the Akron,[15] MIT,[19] and Prague[23] groups decreased rapidly after reaching a peak value, while our master curve in the one-phase region shows a smooth plateau; and (iii) the final size of the polymer chain became a tiny collapsed globule according to the data reported by the MIT and Prague groups. If we examined the peak position and height as shown in Figure 11, the scattering data by the Akron group showed almost the same peak position and height as those by the MIT group, but results by the Prague group had a different peak position and a different height when compared with those reported by others. This discrepancy can perhaps be ascribed to the difference in solvents used. The Prague group used DOP (dioctyl phthalate) as a solvent instead of cyclohexane. Here, we should pay attention to the Prague experiments which intentionally used a very viscous solvent (e.g., at 2 °C $\eta_0 = 295$ cP for DOP). The viscous solvent permitted the Prague group to go down below the cloud-point curve *in the metastable region* without any serious aggregation of polymer coils or fractional separation over relatively short time periods. Thus, the Prague group appeared to be able to measure the static (R_g) and the hydrodynamic (R_h) sizes below the cloud-point curve. However, their thermodynamic condition belonged to the metastable region, not the stable region. Many data in their experiments might never have reached thermodynamic equilibrium. Let us examine more carefully the data reported by the MIT group. First, their values of R_g and R_h with $M_w = 20.6 \times 10^6$ g/mol at the Θ-temperature were reported as respectively $\sim 1.84 \times 10^3$ and $\sim 1.37 \times 10^3$ Å.

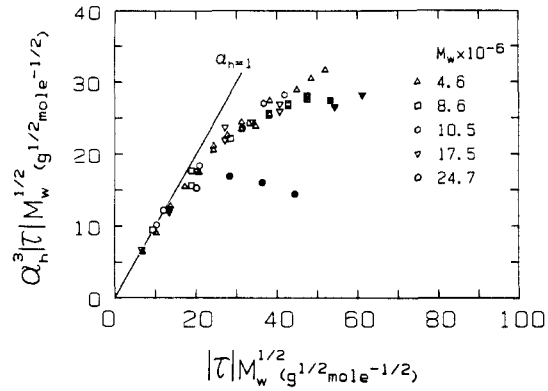

Figure 12. Variation of scaled expansion factor $\alpha_h^3|\tau|M_w^{1/2}$ of hydrodynamic size as a function of scaled reduced temperature $|\tau|M_w^{1/2}$. The asymptotic plateau region has not been observed in this experiment. Data are listed in ref 43. Filled symbols indicate "metastable" collapsed regime. It should be noted that the scaled curve was obtained by using PS with different molecular weights and at different concentrations. One may see a possible leveling in the scaled curve, suggesting that we have almost reached the collapsed regime based upon hydrodynamic size.

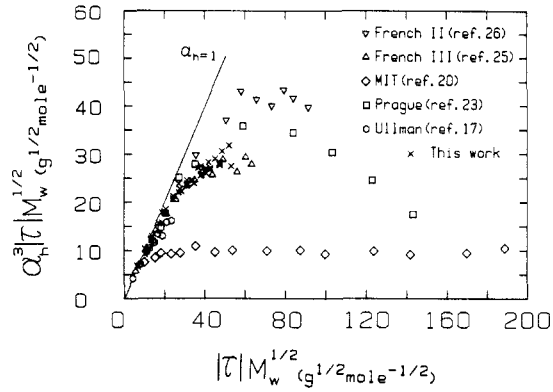

Figure 13. Comparison of our hydrodynamic size data with reference data: (□) DOP (dioctyl phthalate) was used as solvent; (△) intrinsic viscosity was used instead of the translational diffusion coefficient for the calculation of hydrodynamic size.

If R_g^2/M_w and R_h^2/M_w can be used as a polydispersity parameter, we could estimate the polydispersity ($M_w/M_n \sim 1.7 \pm 0.3$) of the MIT sample from Figure 5. This value is much larger than $M_w/M_n = 1.3$ which they indicated. After checking Figure 1 of their article,[19b] which showed a plot of a_1/a_2 (=scattering intensity of solvent/scattering intensity of solute) vs. scattering angle at several different temperatures, we found that the y-intercept kept almost constant with respect to a temperature drop of 3.6 °C from 36.2 to 32.6 °C. However, this intercept decreased by more than ~10% in the next temperature drop of 3.6 °C from 32.6 to 29.0 °C. They explained that this change could be attributed only to the decrease of background scattering from the solvent. According to our calculations, the rate of decrease in a_1/a_2 is only a few percent per 10 °C. The 10% discrepancy seems a little bit larger than the experimental error limits. As already shown in Figure 9, our 17B sample had similar trends in the metastable region, showing abrupt decreases in the y-intercept. Therefore, we spectulate that perhaps some of the data reported by the MIT group were also measured below the cloud-point curve and that they could not recognize the very slow process of phase separation because of the extremely dilute polymer solution concentration which they used. It should be noted that in our time studies of the PS/CY system, we had to examine the angular distribution of absolute scattered intensity changes over periods of weeks for each thermodynamic state before we were able to convince ourselves of the behavior in the metastable region.

VIc. Hydrodynamic Size. Figure 12 shows a plot of the scaled expansion factor $\alpha_h^3|\tau|M_w^{1/2}$ vs. the scaled reduced temperature $|\tau|M_w^{1/2}$. By comparing Figure 12 of the hydrodynamic size with Figure 6 of the static size, we observed the following:

(i) The hydrodynamic size had a wider Θ-regime ($0 < |\tau|M_w^{1/2} < 15$) than the static size had ($0 < |\tau|M_w^{1-2} < 10$), as expected from theory.

(ii) We could not definitively reach the collapsed state based on the hydrodynamic size using the finite concentrations within our experimental capabilities. In fact, a wider Θ-regime already suggests that the collapsed regime based on the hydrodynamic size will be located further away in $|\tau|M_w^{1/2}$ than that based on the static size. It is well-known that in the good solvent limit, hydrodynamic properties of a long polymer chain converge much more slowly to the asymptotic limit than static properties. A guideline to this convergence problem in the poor solvent limit can be obtained from eq 5 and 7 of the blob theory. If we assume only one scaled reduced temperature where the collapsed regime of both static and hydrodynamic sizes are achieved, the ratio $\alpha_h^3|\tau|M_w^{1/2}/\alpha_g^3|\tau|M_w^{1/2}$ should be constant in the collapsed regime, yielding a value of 2.08 for this ratio.

If the approximate blob theory prediction is correct, the value of $\alpha_h^3|\tau|M_w^{1/2}$ in the collapsed regime is supposed to be around 42 (=2.08 × 20.1). In our experiments, we only reached a value of ~30 for $\alpha_h^3|\tau|M_w^{1/2}$. If the polymer chain in the collapsed state is viewed as a solidlike dense hard sphere (though we do not believe that this possibility is correct in our case), the ratio will increase to 7.33, corresponding to an asymptotic $\alpha_h^3|\tau|M_w^{1/2}$ value of ~146.

(iii) Our data in the metastable region shows similar behavior in both static (R_g) and hydrodynamic (R_h) properties (see filled symbols in Figures 6 and 12).

(iv) Except for data in the metastable region, all our results can be represented by a master curve. Our hydrodynamic data were compared with the literature results in Figure 13. Although claims were made that the collapsed state based on the hydrodynamic size was observed, the asymptotic heights at the plateau region were all different. For example, the $\alpha_h^3|\tau|M_w^{1/2}$ heights reported by the French II,[26] French III,[24,25] and MIT[19] groups were, respectively, 42, 30, and 10 as shown in Figure 13. Why could they reach the collapsed regime based on the hydrodynamic size while we could not? Or did they? First, we checked the data reported by the French II group. Data points in the collapsed regime were obtained mainly from measurements using a Toyo Soda sample ($M_w = 20.6 \times 10^6$ g/mol; $C = 2.1 \times 10^{-5}$ g/mL) from 31.5 to 28.8 °C. According to our measurements, this Toyo Soda sample has $M_w = 20 \times 10^6$ g/mol, $M_w/M_n \sim 2$, and $R_g^2/M_w \sim 15.0 \times 10^{-18}$ cm^2 (mol/g). Therefore, the polydispersity index of this sample is comparable with that of our sample 17B ($M_w/M_n \sim 2.1$). If we remember that a polymer solution of 17B with $C = 1.8 \times 10^{-6}$ g/g was eventually phase separated at 30.5 °C, the data reported by the French II group measured around 30 °C with $C = 2.1 \times 10^{-5}$ g/mL might correspond to measurements in the metastable region. In the previous section, we already discussed the possibility that the data reported by the MIT group might also be measured in the metastable region. Thus, a slowly increasing function of $\alpha_h^3|\tau|M_w^{1/2}$ with respect to $|\tau|M_w^{1/2}$ could become apparently flat before the decrease. We need more experiments using monodisperse high molecular weight polymer samples over a wider temperature range in order to convince ourselves of the achievement of a real

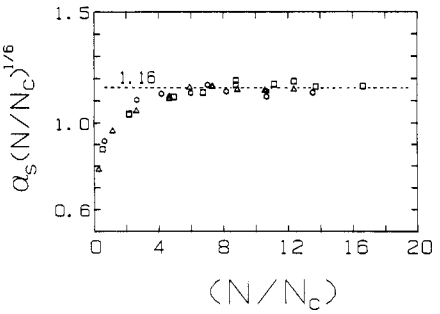

Figure 14. Universal plot of static size vs. reduced blob parameter (N/N_c). All data obtained from different molecular weight polystyrene samples could be superposed on one curve: (△) sample 4N, $M_w = 4.6 \times 10^6$ g/mol; (□) sample 8N, $M_w = 8.6 \times 10^6$ g/mol; (○) sample F-3, $M_w = 10.5 \times 10^6$ g/mol. Data points reached an aymptotic collapsed value (1.16) predicted by eq 5 above $N/N_c > 5$. N/N_c is the number of temperature blobs in a single polymer chain with N_c being the number of segments in a temperature blob. It should be noted that we have used the A^*N_1 value based on eq 18 and the experimental asymptotic height in Figure 6.

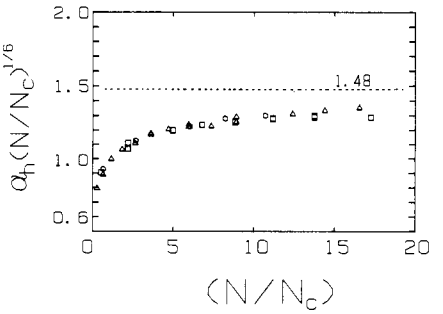

Figure 15. Universal plot of hydrodynamic size vs. reduced blob parameter (N/N_c). Although all data points could be superimposed, they did not reach an asymptotic collapsed value (1.48) of eq 7. Symbols are the same as in Figure 14. N/N_c is the number of temperature blobs in a single polymer chain. The same value of A^*N_1 reported in Figure 15 (based on static size) was used.

collapsed state based on the hydrodynamic size. In Figure 13, the hydrodynamic size reported by the French III group was calculated from the intrinsic viscosity $[\eta]$ instead of the translational diffusion coefficient. By using the Einstein equation of viscosity, another hydrodynamic size R_η is given as $R_\eta^3 \sim M[\eta]$. The expansion factor of the intrinsic viscosity α_η^3 is defined as $\alpha_\eta^3 = [\eta]/[\eta]_\Theta$, where $[\eta]_\Theta$ and $[\eta]$ are respectively the intrinsic viscosity at the Θ-temperature and that at a given temperature. As $\alpha_h^3|\tau|M_w^{1/2}$ values based on our hydrodynamic size determinations show very good agreement with those of $\alpha_\eta^3|\tau|M_w^{1/2}$ reported by the French III group, α_η^3 is simply scaled as α_h^3 at least in the temperature range of our studies. Weill and des Cloizeaux[49] reported that in the expanded coil, the expression $\alpha_\eta^3 = \alpha_s^2\alpha_h$ can describe the reality of R_η better than the perturbation expansion of α_s and α_h.

In order to construct a more universal plot, the reduced blob parameter N/N_c should be used as the x-axis instead of the scaled reduced temperature $|\tau|M_w^{1/2}$. We recall that the reduced blob parameter is directly related to $|\tau|M_w^{1/2}$ with

$$\frac{N}{N_c} = \frac{\tau^2 M_w}{M_0(A^*N_1)} \tag{17}$$

where M_0 is the molecular weight (104 g/mol) of one monomer and N_1 is the number of monomer units in a statistical length.

According to Ackasu and Han,[29] the product (A^*N_1) cannot be obtained from theory but becomes an adjustable parameter between theory and experiment. The prefactor (A^*N_1) should be determined empirically by fitting the experimental data to the theory. By combining static experimental results in the collapsed regime, $\alpha_s^3|\tau|M_w^{1/2} = 20.1$, and the theoretical expectation of eq 5, we have

$$\frac{N}{N_c} = \frac{\tau^2 M_w}{104(1.6)} \tag{18}$$

The value of our prefactor ($A^*N_1 \sim 1.6 \pm 0.3$) was much smaller when compared with the value ($A^*N_1 \sim 4.0$) estimated by Ackasu and Han in the good solvent regime but in good agreement with the value ($A^*N_1 \sim 1.6$) reported by the French II group. This agreement comes from the fact that their hydrodynamic asymptotic height ($\alpha_h^3|\tau|M_w^{1/2} \sim 42$) is very close to the theoretically calculated value ($\alpha_h^3|\tau|M_w^{1/2} \sim 41.8$) based on our static asymptotic height ($\alpha_s^3|\tau|M_w^{1/2} \sim 20.1$).

If we assume that the segment numbers in one statistical length N_1 remain constant in both good and poor solvent regimes, only A^* should be a temperature-dependent parameter. We shall discuss this point in a later article.[50] Figures 14 and 15 are universal plots of $\alpha_s(N/N_c)^{1/6}$ and $\alpha_h(N/N_c)^{1/6}$ vs. the reduced blob parameter N/N_c, respectively. In Figure 14, $\alpha_s(N/N_c)^{1/6}$ reached an asymptotic value (1.16) above $N/N_c > 5$. However, Figure 15 shows us that the asymptotic value (1.48) based on the hydrodynamic size is still inaccessible by us at this moment as discussed before.

VId. Solvent Permeability. Coil-to-globule transition of a single polymer chain is related to a variation of monomer density distribution inside the chain as well as a contraction in polymer size. According to the theoretical prediction of the collapsed state, the monomer density distribution should be uniform. In other words, there should exist a uniform monomer density distribution whenever a collapsed state is achieved. This implies that the two physical quantities of monomer density distribution and polymer size are dependent upon each other. Now we introduce another physical quantity, which may be affected by the coil-to-globule transition. The solvent permeability is related to the amount of solvent existing inside the polymer chain. There are two experimental parameters which can show solvent permeability. One is the ratio of hydrodynamic size to static size (R_h/R_g), the other being f in eq 13 of $\bar{\Gamma}/K^2$ vs. K^2. If attractive interactions are strong enough to contract the polymer chain down to a collapsed globule whose density is close to that of a solid polymer ball (the limit of solvent impermeability), this globular chain has $R_h/R_g = 1.29$. However, the blob theory predicts that the ratio R_h/R_g varies from 0.664 at the Θ-temperature to 0.848 in the poor solvent limit. Lately, Allegra et al.[14] reported that this ratio becomes 1.08 if the globule were assumed to be fully solvent permeable but still retaining a uniform monomer density. In Figure 16, the normalized ratio $(R_h/R_g)/(R_h/R_g)_\Theta$ was plotted against the scaled reduced temperature $|\tau|M_w^{1/2}$. The data points used in Figure 16 were calculated from two master curves of hydrodynamic and static size (see Figures 6 and 12). As shown in Figure 16, the normalized ratio increased only a few percent over the entire range of $0 < |\tau|M_w^{1-2} < 50$ and is still far away from the blob theory value 1.27 (=0.846/0.664). On the basis of this observation, we suggest that the solvent permeability at the collapsed state based on static size measurements is almost the same as that of a Gaussian random coil at the Θ-temperature. It is well-known that the f value is zero for a monodisperse hard sphere. The variation of f values during the coil-

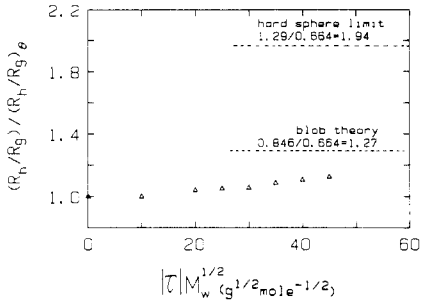

Figure 16. Variation of normalized R_h/R_g ratio as a function of scaled reduced temperature ($|\tau|M_w^{1/2}$). The normalized ratio has increased by only ~10% even at the collapsed regime based upon the static R_g values and is far away from the value predicted by means of eq 5 and 7 in the blob theory.

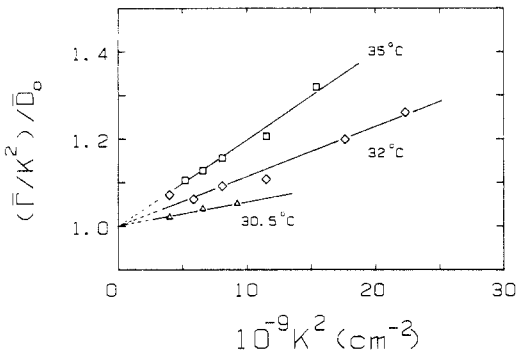

Figure 17. Plots of $\bar{\Gamma}_N/K^2$ [$=(\bar{\Gamma}/K^2)/D_0$] versus K^2 at several different temperatures: sample 17B, $M_w = 17.5 \times 10^6$ g/mol); $C = 1.8 \times 10^{-6}$ g/g. As the temperature is cooled down, the slope becomes smaller.

to-globule transition indicates a degree of solvent permeability. Experimentally the f value can be estimated from the slope of $\bar{\Gamma}/K^2$ vs. K^2, the translational diffusion coefficient at infinite dilution, and the radius of gyration by using eq 19. Figure 17 shows the angular dependence

$$f = (\text{slope})/(\bar{D}_0 R_g^2) \tag{19}$$

of normalized $\bar{\Gamma}_N/K^2$ [$=(\bar{\Gamma}/K^2)/\bar{D}_0$] as a function of K^2 at various temperatures. With the value of R_g at each temperature, the f value can be calculated from the slope in a plot of $\bar{\Gamma}/K^2$ vs. K^2. Figure 18 shows a plot of f as a function of the scaled reduced temperature. We can again observe that the solvent permeability does not vary even in the collapsed state based on static size. However, for data corresponding to the metastable region, the f value drops toward zero. This means that in the metastable region, the solvent permeability decreases rapidly.

VII. Conclusions

Measurements of both the radius of gyration and the hydrodynamic radius in a single polymer chain have been performed in the PS/CY system below the Θ-temperature. Contraction of a polymer coil having different molecular weights at various temperatures could be represented by master curves of static and hydrodynamic sizes. The collapsed regime based on the static size was reached at $|\tau|M_w^{1/2} > 30$ with the asymptotic height $\alpha_s^3|\tau|M_w^{1/2} \sim 20$ in a plot of $\alpha_s^3|\tau|M_w^{1/2}$ vs. $|\tau|M_w^{1/2}$. However, the collapsed regime based on the hydrodynamic size could not be achieved definitively with our present instrumentation and PS samples. In order to investigate thoroughly the slower convergence of the hydrodynamic size to the collapsed regime, we need more conclusive experimental data of very high molecular weight polymer samples with narrower indices of polydispersity ($M_w/M_n < 1.3$). We could explain

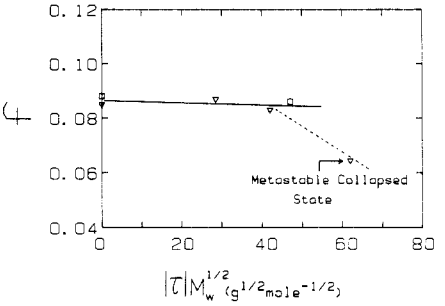

Figure 18. Variation of f value as a function of scaled reduced temperature ($|\tau|M_w^{1/2}$). The f value was almost constant over the whole temperature range except in the metastable collapsed regime: (□) sample 8N, $M_w = 8.6 \times 10^6$ g/mol, $C = 9.6 \times 10^{-6}$ g/g; (▽) sample 17B, $M_w = 17.5 \times 10^6$ g/mol, $C = 1.8 \times 10^{-6}$ g/g.

the discrepancies reported in the literature and our time-dependent experimental data, as shown in Figures 16 and 18, by invoking phase separation and aggregation in the two phase metastable region. For polystyrene in cyclohexane, the coil-to-globule transition is diffuse. Solvent permeability is proposed as an additional variable to the polymer size and the monomer density distribution. From experimental results of the R_h/R_g ratio and f value, we conclude that based on static size, solvent permeability in the polymer coil does not change appreciably from Gaussian coil to the collapsed globule.

Acknowledgment. We gratefully acknowledge support of this research work by the National Science Foundation, Polymers Program (DMR 8617820), and the U.S. Department of Energy (DEFG0286ER45237).

Registry No. Polystyrene, 9003-53-6; cyclohexane, 110-82-7.

References and Notes

(1) Flory, P. J. *Principle of Polymer Chemistry*; Cornell University: Ithaca, NY, 1952.
(2) Ptitsyn, O. B.; Kron, A. K.; Eizner, Y. Y. *J. Polym. Sci., Polym. Phys. Ed.* **1968**, *16*, 3509.
(3) Eizner, Y. Y. *Polym. Sci. USSR (Engl. Transl)* **1972**, *14*, 1695.
(4) Domb, C. *Polymer* **1974**, *15*, 259.
(5) Massih, A. R.; Moore, M. A. *J. Phys. A: Math. Gen.* **1975**, *8*, 237.
(6) de Gennes, P.-G. *J. Phys. Lett.* **1975**, *36*, L55; **1978**, *36*, L299.
(7) Moore, M. A. *J. Phys. A: Math Gen.* **1977**, *10*, 305.
(8) Post, C. B.; Zimm, B. H. *Biopolymers* **1979**, *18*, 1487; **1982**, *21*, 2123.
(9) Sanchez, I. C. *Macromolecules* **1979**, *12*, 980.
(10) Williams, C.; Brochard, F.; Frisch, H. L. *Annu. Rev. Phys. Chem.* **1981**, *32*, 433.
(11) Allegra, G.; Ganazzoli, F. *Macromolecules* **1983**, *16*, 1311.
(12) DiMarzio, E. A. *Macromolecules* **1984**, *17*, 969.
(13) Kholodenko, A. L.; Freed, K. F. *J. Chem. Phys.* **1984**, *80*, 900.
(14) Allegra, G.; Ganazzoli, F. *J. Chem. Phys.* **1985**, *83*, 397.
(15) Slagowski, E.; Tsai, B.; McIntyre, D. *Macromolecules* **1976**, *9*, 687.
(16) Nierlich, M.; Cotton, J. P.; Farnoux, B. *J. Chem. Phys.* **1978**, *69*, 1379.
(17) Bauer, D. R.; Ullman, R. *Macromolecules* **1980**, *13*, 392.
(18) Pritchard, M. J.; Caroline, D. *Macromolecules* **1980**, *13*, 957.
(19) (a) Swislow, G.; Sun, S. T.; Nishio, I.; Tanaka, T. *Phys. Rev. Lett.* **1980**, *44*, 796. (b) Sun, S. T.; Nishio, I.; Swislow, G.; Tanaka, T. *J. Chem. Phys.* **1980**, *73*, 5971.
(20) Miyaki, Y.; Fujita, H. *Polym. J.* **1981**, *13*, 749.
(21) Oyama, T.; Shiokawa, K.; Baba, K. *Polym. J.* **1981**, *13*, 167.
(22) Post, C. B.; Zimm, B. H. *Biopolymers* **1982**, *21*, 2139.
(23) Stepanek, P.; Konak, C.; Sedlacek, B. *Macromolecules* **1982**, *15*, 1214.
(24) Perzynski, R.; Adam, M.; Delsanti, M. *J. Phys.* **1982**, *43*, 129.
(25) Perzynski, R.; Delsanti, M.; Adam, M. *J. Phys.* **1984**, *45*, 1765.
(26) Vidakovic, P.; Rondelez, F. *Macromolecules* **1984**, *17*, 418.
(27) Selser, J. C. *Macromolecules* **1985**, *18*, 585.
(28) Daoud, M.; Pincus, P.; Stockmayer, W. H.; Witten, T., Jr. *Macromolecules* **1983**, *16*, 1833.
(29) Ackasu, A. Z.; Han, C. C. *Macromolecules* **1979**, *12*, 276.
(30) Daoud, M.; Jannink, G. *J. Phys.* **1978**, *39*, 331.
(31) Farnoux, B.; et al. *J. Phys.* **1978**, *39*, 77.

(32) *Light Scattering from Polymer Solutions*; Huglin, M. G., Ed. Academic: New York, 1972.
(33) *Photon Correlation and Light Beating Spectroscopy*; Cummins, H. Z., Pike, E., Eds.; Plenum: New York, 1974.
(34) Chu, B. *Laser Light Scattering*; Academic: New York, 1974.
(35) *Dynamic Light Scattering*; Berne, B. J., Pecora, P., eds.; Wiley: New York, 1976.
(36) Koppel *J. Chem. Phys.* **1972**, *57*, 4814.
(37) Stockmayer, W. H.; Schmidt, M. *Pure Appl. Chem.* **1982**, *54*, 407.
(38) Brown, J. C.; Pusey, P. N. *J. Phy. D* **1974**, *7*, L31.
(39) *Polymer* Handbook; Bandrup, J., Immergut, E. H., Eds.; Wiley: New York, 1975.
(40) Ehl, J.; Loucheux, C.; Reiss, C.; Benoit, H. *Makromol. Chem.* **1964**, *75*, 35.
(41) Timmermans, J. *Physico-chemical Constants of Pure Organic Compounds*; Elsevier: New York, 1950.
(42) Miyaki, Y.; Einaga, Y.; Fujita, H. *Macromolecules* **1978**, *11*, 1180.
(43) Park, I. H. Ph.D. Thesis, SUNY/Stony Brook, 1986.
(44) Outer, P.; Carr, C. I.; Zimm, B. H. *J. Chem. Phys.* **1950**, *18*, 830.
(45) Schmidt, M.; Burchard, W. *Macromolecules* **1981**, *14*, 210.
(46) Lee, S. P.; Tscharnuter, W.; Chu, B.; Kuwahara, N. *J. Chem. Phys.* **1972**, *57*, 4240.
(47) Cuniberti, C.; Bianchi, U. *Polymer* **1974**, *15*, 346.
(48) de Gennes, P.-G. *J. Phys. Lett.* **1975**, *36*, L55.
(49) Weill, G.; des Cloizeaux, J. *J. Phys.* **1979**, *40*, 99.
(50) Chu, B.; Park, I. H.; Wang, Q.-W.; Wu, C. *Macromolecules*, part 2 of this series, in press.

Structural Studies of Phase Transitions in Poly(di-*n*-alkylsiloxanes). 1. Poly(dimethylsiloxane) and Poly(diethylsiloxane)

J. Friedrich† and J. F. Rabolt*

IBM Almaden Research Center, San Jose, California 95120. *Received October 25, 1986*

ABSTRACT: Raman studies of poly(dimethylsiloxane) [PDMS] and poly(diethylsiloxane) [PDES] have been carried out from room temperature to −263 °C (10 K). Several bands characteristic of either the backbone or the allyl side chains have been identified and their bandwidth and frequency position followed as a function of temperature. A number of phase transitions, initially observed by DSC measurements, have been evaluated in terms of the molecular mobility introduced into the backbone and side chain at the transition temperature. In the case of PDES, the low-temperature transition (−60 °C) can be classified as an order–disorder transition leading to the formation of a "condis" crystal.

Introduction

The chemical incorporation of mesogenic groups into the backbone and side chain of long-chain polymers has led to the generation of a large number of liquid crystalline polymers,[1,2] which exhibit both novel molecular structures and unique functional properties. Whereas much of the focus of recent scientific activities has been on the latter, few comprehensive structural studies of liquid crystalline polymers have appeared. The motivation for such investigations lies in the fact that the characterization of the conformational, crystal, and morphological structure responsible for liquid crystalline behavior will provide a general understanding of the role of these parameters on mesogenic activity.

From a structural point of view the poly(di-*n*-alkylsiloxanes) have received a considerable amount of attention over the past 10 years. Although one of the simplest of these structures, poly(dimethylsiloxane) (PDMS) shows no liquid crystalline properties,[3,4] it has been the subject of a considerable amount of theoretical and experimental interest.[3-7]

Poly(di-*n*-ethylsiloxane), on the other hand, has been shown to exhibit a crystal–crystal transition and at least one liquid crystalline phase.[8-12] Pochan et al.[8] have investigated all three transitions by DSC, NMR, WAXD, optical microscopy, and light scattering methods and have concluded that the high-temperature phase exists as a "viscous crystalline" phase and is a composite of a partially ordered and a totally amorphous phase. More recent work by Papkov et al.[4] and Tsvankin et al.[3] has used WAXD and SAXS to determine that PDES is polymorphic, existing in either a monoclinic and/or a tetragonal form depending on the thermal history. Each of these forms independently showed a low-temperature transition in the −83 to −63 °C (190–210 K) range that did not involve a dramatic change in crystal structure, i.e., the monoclinic form remained monoclinic while the tetragonal polymorph also retained its structure above the low-temperature phase transition. The primary changes that occur at −83 to −63 °C (190–210 K) are in the *a* and *b* dimensions of the unit cell which is accompanied by a drop in the crystalline density. A further lowering[3] of the density was observed to occur in the 7–27 °C (280–290 K) range but in this case was attributed to a transition from the monoclinic and tetragonal polymorphs to a mesomorphic phase.

Vibrational spectroscopy has shown considerable promise in studying molecular motion in polymers due to the extent of information available through studies of peak position, bandwidth, and band intensity as a function of temperature. In the low-frequency (100–600-cm^{-1}) region[13,14] of nonlocalized vibrations, information about conformational disorder can be obtained while in the higher frequency regions an assessment of localized molecular motion should be possible. It was this capability to use bandwidths and peak intensities to describe the overall picture of the temperature-induced phase transitions in PDMS and PDES that motivated this study.

Experimental Section

All Raman spectra were obtained with a Spectra Physics 165-08 argon ion laser operating at wavelengths of either 488.0 or 514.5 nm with a power level of 0.1–0.2 W. Light scattered at 90° to the incident laser direction was collected and focused into a Jobin-Yvon Ramanor HG2S double monochromator equipped with an RCA 31034A-02 cooled photomultiplier and standard photon-counting electronics. Data from multiple scans were

† Permanent address: Experimental Physik IV, Universitat Bayreuth, D-8580 Bayreuth, West Germany.

0024-9297/87/2220-1975$01.50/0